Dalton Transactions

Accepted Manuscript

ROYAL SOCIETY OF CHEMISTRY

www.rsc.org/dalton

Journal Name

ARTICLE

Tuning of intramolecular charge transfer properties and charge distributions in ferrocene-appended catechol derivatives by chemical substitution

Received 00th January 20xx,
Accepted 00th January 20xx

DOI: 10.1039/x0xx00000x

www.rsc.org/

Keishiro Tahara,[a,] * Shogo Akehi,[a] Tetsuhiro Akita,[a] Shohei Katao,[a] Jun-ichi Kikuchi,[a,] * and Ken Tokunaga[b]

In this study, we report intramolecular charge transfer (ICT) properties and charge distributions in a series of FcC derivatives (FcC = 4-ferrocenylcatecholate where Fc = ferrocene and C = catecholate). This series consists of a previously reported complex FcV (4-ferrocenylveratrole) and newly synthesized complexes FcA (4-ferrocenylcatechol *bis*(acetate) and Pt(^{t}Bu$_2$bpy)(FcC) (^{t}Bu$_2$bpy = 4,4′-di-*tert*-butyl-2,2′-dipyridyl). An electrochemical analysis of Pt(^{t}Bu$_2$bpy)(FcC) using cyclic voltammetry revealed two well-defined, reversible waves which were assigned to the sequential oxidation of the Pt(^{t}Bu$_2$bpy)(C) and Fc moieties. The potential splitting between the waves (524 mV) indicated that there was an electronic interaction between both moieties. The intramolecular charge transfer (ICT) property and charge distribution of [Pt(^{t}Bu$_2$bpy)(FcC)]$^{\bullet+}$ were rationalized by comparison with the [FcV]$^{\bullet+}$ and [FcA]$^{\bullet+}$ (4-ferrocenylcatechol *bis*(acetate)). DFT calculations and UV-vis-NIR spectroscopy revealed that [Pt(^{t}Bu$_2$bpy)(FcC)]$^{\bullet+}$, [FcV]$^{\bullet+}$, and [FcA]$^{\bullet+}$ were ferrocenium (Fc$^+$)-centered rather than semiquinone ligand-centered and that these complexes exhibited ICT transition bands from the catechol-derivatized framework to the Fc$^+$ moiety in the near infrared (NIR) region. Both the electronic coupling parameter (H_{AB}) and delocalization parameter (α) increased in value as the electron-donating strength of the substituent groups in the catechol-derivatized framework increased (OCOCH$_3$ ([FcA]$^{\bullet+}$) < OCH$_3$ ([FcV]$^{\bullet+}$) < O$^-$ ([Pt(^{t}Bu$_2$bpy)(FcC)]$^{\bullet+}$)). The electronic interactions between the organometallic center and the non-innocent framework were tuned by changing the substituents. The potential energy surfaces of the Fc$^+$ derivatives, obtained using two-state Marcus-Hush theory, can be modulated by changing the energy level of the molecular orbitals of the appended catechol-derivatized moieties.

Introduction

Valence tautomeric (VT) complexes are composed of redox-active ligands and transition metal ions.[1, 2] VT complexes can acquire more than two stable electronic states, which can be mutually accessed by intramolecular electron transfer (IET) induced by absorption of photons and changes in temperature and/or pressure. Efforts to connect IET phenomena at a molecular level to switching functions at a macroscopic level, for use in molecular electronics, have been reported, especially for cobalt catecholate complexes.[2-4] Switchable molecular devices require a single-bistability, that is, two stable electronic states between which the system can switch in response to physical stimuli.[4] However, more elaborate devices require multi-bistability, that is, three or more stable electronic states in which the system can switch among.[5] A promising approach to realize these complicated systems is the use of transition metal ions in which a number of different valence states are accessible. An example of a three-membered VT interconversion was demonstrated in a manganese catecholate complex capable of acquiring the Mn (IV) state.[6] Alternative approaches include the design of new ligands that can provide a third stable electronic state and control the energy differences between stable electronic structures, IET directions, and charge distributions in VT complexes.

VT complexes are composed of not only redox-active ligands and transition metal ions but also larger redox-active units. Ferrocene (Fc) has been covalently linked to redox-active units to probe IET phenomena.[7, 8] The resulting Fc conjugates are attractive redox-active materials as the redox behavior of Fc is reversible, stable, and the Fe(III)/Fe(II) redox-couple has a low potential. Additionally, Fc has been reported to donate electrons to quinone/semiquinone/hydroquinone redox systems.[9] These Fc conjugates are attractive candidates for the study of IET phenomena in which proton transfer and hydrogen-bonding accompanies the redox event. To the best of our knowledge, transition metal complexes, in which a catecholate ligand is covalently linked to a cyclopentadienyl (Cp) of Fc, have not been reported. We have reported the synthesis of 4-ferrocenylveratrole (**1**, FcV) and 4,6-diferrocenylveratrole (**2**, FcVFc) (Chart 1a) as precursors to 4-ferrocenylcatechol (FcC) and 4,5-diferrocenylcatechol (FcCFc), respectively (V =

[a] *Graduate School of Materials Science, Nara Institute of Science and Technology, 8916-5, Takayama, Ikoma,6300192, Japan.*
[b] *Division of Liberal Arts, Kogakuin University, 2665-1, Nakano, Hachioji, Tokyo 1920015, Japan.*
Electronic Supplementary Information (ESI) available: Characterization of new compounds, UV-vis-NIR spectra of oxidized species, DFT calculation data. CCDC 987989, 987990, 987994. See DOI: 10.1039/x0xx00000x

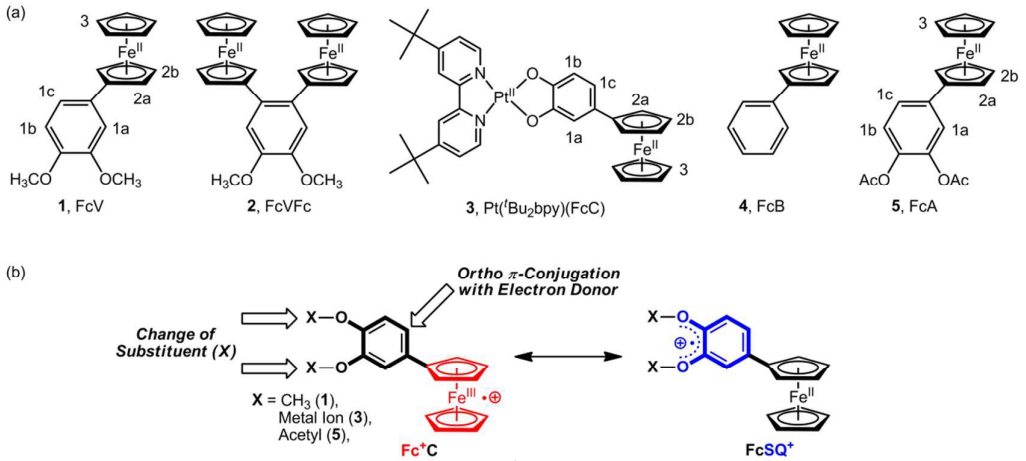

Chart 1. (a) Structures of Fc derivatives and atom numbering used for ^{1}H-NMR assignments. (b) Strategy to tune the charge distribution and ICT properties between Fc^+C and $FcSQ^+$ electronic states and probe the effect of *ortho* π-conjugation on ICT properties.

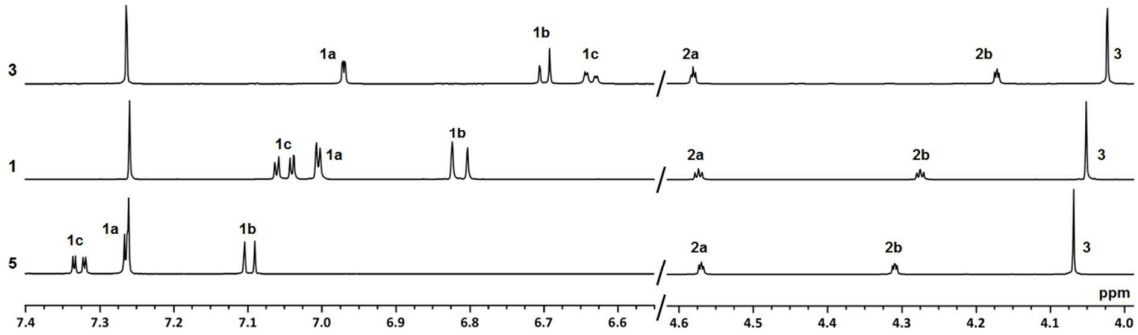

Figure 1. Partial ^{1}H-NMR spectra of **1**, **3**, and **5** in $CDCl_3$.

veratrole (1,2-dimethoxybenzene); C = catechol (or catecholate)), and demonstrated their use in borate complexes.[10] In this study, we report intramolecular charge transfer (ICT) properties and charge distributions in a series of FcC derivatives. To tune the interconversion between the Fc^+C and $FcSQ^+$ electronic states (SQ = semiquinone), we chemically modified the FcC derivatives at the O atoms by changing the substitution groups, as well as by metal complexation (Chart 1b). To ensure that the Fc^+C and $FcSQ^+$ electronic states were dominant, Pt(^{t}Bu$_2$bpy)(FcC) (**3**) (^{t}Bu$_2$bpy = 4,4′-di-*tert*-butyl-2,2′-dipyridyl) was synthesized and characterized. Pt(^{t}Bu$_2$bpy)(C) was selected as a component of the transition metal complex in **3**, as closely related analogues are predominantly oxidized on the C moieties with only a minor contribution from the Pt(II) d orbitals.[11] In addition, the oxidation potentials of the components of Fc and related Pt(II) catecholate complexes are very close, which is advantageous for an electronic interaction between the Fc and C moieties.[12] To understand the ICT properties of FcC in $\mathbf{3}^+$, we compare its charge distribution, ICT direction, and electronic coupling to the ferrocenyl complexes **4** (X = CH_3) and **5** (X = acetyl, Ac) (Chart 1a). The effect of *ortho* π-conjugation, caused by an additional Fc group in complex $\mathbf{2}^+$, on the ICT properties is also reported.

Results and discussion

Synthesis and characterization of Fc derivatives

BBr_3 mediated demethylation of complex **1** followed by complexation to Pt(^{t}Bu$_2$bpy)Cl_2 gave **3** in 71% yields (Scheme 1). FcC was not stable in air as reported elsewhere,[9c] however direct use of the crude product under a N_2 atmosphere was effective to synthesis and isolate **3**. In contrast, complex **3** was stable in air once the catecholate ligand was coordinated to the Pt center. A reference compound containing acetyl groups (**5**) was synthesized by condensation of the crude catechol with acetic anhydride. Compounds **3** and **5** were characterized by ^{1}H- and ^{13}C-NMR spectroscopy and ESI-MS (Figures S1 to S5). The ^{1}H-NMR spectra of the Fc compounds in $CDCl_3$, displaying the relevant regions, are shown in Figure 1. The proton signals of the phenyl (1a, 1b, and 1c, Chart 1a) and Cp rings (2b and 3, Chart 1a) were shifted upfield as the electron-donating strength of the substituents[13] on the phenyl rings increased ($OCOCH_3$ < OCH_3 < O^-). Differential NOE spectroscopy revealed an enhancement of 7.9% for the 2a proton upon irradiation at the 1a proton (Figure S6). This was consistent with the H···H distances (9H···36H and 30H···38H) in the DFT-optimized structure of Pt(bpy)(FcC) (**3'**), in which the ^{t}Bu$_2$bpy group of **3** was replaced by bpy (2,2′-dipyridyl); the phenyl and Cp rings were almost coplanar in **3'** (Figure 2 and Table S3). Compound **1** exhibited similar NOE enhancements (8.7% in $CDCl_3$) (Figure S6) to those of compound **3**, indicating a common planarity was present in the series of Fc compounds.

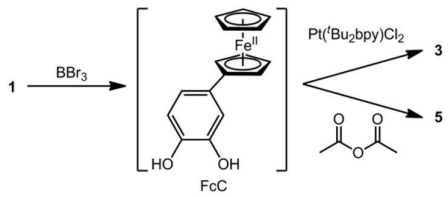

Scheme 1. Synthesis of **3** and **5**.

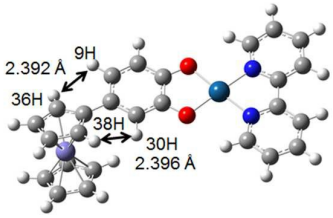

Figure 2. DFT-optimized structures of Pt(bpy)(FcC) with IEFPCM (CH_2Cl_2).

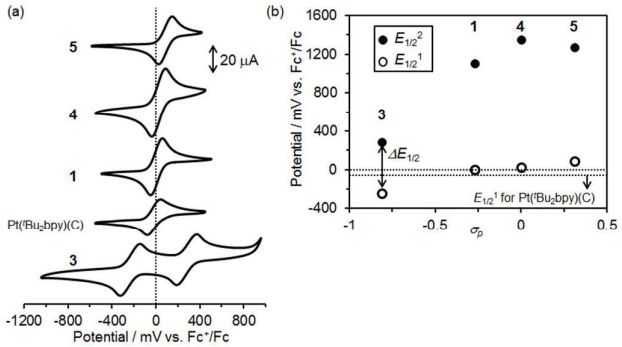

Figure 3. (a) Cyclic voltammograms of **1**, **3**, **4**, **5**, and Pt(^{t}Bu$_2$bpy)(C) (1.0 mM) in CH_2Cl_2 containing ^{n}Bu$_4$NPF$_6$ (0.1 M). Scan rate: 100 mV s^{-1}. (b) Plot $E_{1/2}{}^1$ and $E_{1/2}{}^2$ potentials for **1**, **3**, **4**, and **5** against the Hammett *para* parameter.

Table 1. Electrochemical data for Fc derivatives.[a]

compound	$E_{1/2}{}^1$	$E_{1/2}{}^2$	$\Delta E_{1/2}$	$\sigma_p{}^c$
1	5[b]	1105[e]	1100	–0.27
2	–77[b]	90[e]	167	–0.27
3	–242	282	524	–0.81[d]
4	25	1375[e]	1350	0
5	86	1359[e]	1273	0.31
Pt(^{t}Bu$_2$bpy)(C)	–30	1017[e]	1047	-

[a]Potentials in mV vs. Fc$^+$/Fc. In CH_2Cl_2 (1.0 mM) containing 0.1M ^{n}Bu$_4$NPF$_6$. [b]Previous work (Ref 10). [c]Hammett *para* parameter of the substituents on the phenyl ring (Ref 13). [d]Value for phenolate (Ref 13). [e] $E_{ox}{}^2$ values were adopted because irreversible waves were observed.

Electrochemical behavior of Fc derivatives

The electrochemical behavior of the Fc compounds was investigated using cyclic voltammetry (CV). All measurements were performed in CH_2Cl_2 containing ^{n}Bu$_4$NPF$_6$ as the electrolyte at 298 K (Figure 3a). The redox potentials are listed in Table 1. Complexes **1**, **4**, and **5** displayed a reversible wave ($E_{1/2}{}^1$) corresponding to oxidation of the Fc groups. The $E_{1/2}{}^1$ values decreased as the electron-donating strength of the *para*-substituents on the phenyl groups[13] increased as shown in a Hammett plot (Figure 3b). The second redox wave for complexes **1**, **4**, and **5** corresponding to oxidation of the $C_6H_3O_2X_2$ moiety was not reversible. As such, we examined the one-electron-oxidized species formed by chemical oxidation.

Complex **3** exhibited two well-defined reversible waves, indicating sequential oxidation of the Pt(^{t}Bu$_2$bpy)(C) and Fc moieties and the formation of the one- and two-electron oxidized species **3**$^+$ and **3**$^{2+}$, respectively (Figure 3a and Table 1). In contrast, the difference in the $E_{1/2}$ values between the separate Fc and Pt(^{t}Bu$_2$bpy)(C) complexes was small (30 mV), consistent with previous reports.[12] The low $E_{1/2}{}^1$ value for **3** cannot be explained by substituent effects (Figure 3b). The $E_{1/2}{}^1$ and $E_{1/2}{}^2$ values for **3** were 212 mV lower and 312 mV higher than for the $E_{1/2}{}^1$ value for Pt(^{t}Bu$_2$bpy)(C), respectively, while the $E_{1/2}{}^1$ and $E_{1/2}{}^2$ value for **3** was 242 mV lower and 282 mV higher than the $E_{1/2}{}^1$ value for Fc, respectively. These results indicated that the large potential splitting (524 mV) observed in **3** was caused by an electronic interaction between the Pt(^{t}Bu$_2$bpy)(C) and Fc moieties. Indeed, the catecholate and Fc moieties in complex **3** contributed 77% and 12% to the HOMO, respectively (Figure S15). The potential splitting value for **3** was 494 mV larger than the difference between the $E_{1/2}$ values (30 mV) of the separate Pt(^{t}Bu$_2$bpy)(C) and Fc compounds, highlighting the thermodynamic stability of **3**$^+$ with a comproportionation constant (K_c) of 7.2 × 10^8. Notably, the potential splitting value for **3** was 3.1 times larger than of **2**, which exhibits an inter-Fc interaction *via ortho* π-conjugation in the veratrole framework.

DFT calculations

The optimized geometry, electronic structure, and charge distribution of complex **3**$^+$ were determined using DFT calculations. The solvent effects of CH_2Cl_2 were considered with the IEFPCM approach. The optimized structure of [Pt(bpy)(FcC)]$^{\bullet+}$ (**3'**$^+$) showed the phenyl and Cp rings being coplanar (Figure 4a and Table S3). This was also observed in the optimized structure of the neutral form. The H···H distances (9H···36H and 30H···38H) in **3'**$^+$ were comparable to the neutral form. The natural population analysis (NPA) charges of the Fc fragment in **3'** were close to zero (Table 2). The NPA charges of the Fc and C fragments in **3'**$^+$ increased by 0.761 and 0.177, respectively, when compared with those of **3'** (Figure 4a). This suggested that the first oxidation of **3** occurred largely on the Fc fragment with a partial contribution from the C fragment to the oxidation, and that the positive charge of **3**$^+$ was delocalized largely on the Fc fragment and partly on the C fragment. Such delocalization of the positive charges was in good agreement with the delocalization of the lowest unoccupied molecular orbital (LUMO) (120β) between the Fc and C fragments (Figure 5a and Table 3). On the other hand, the contribution of the Pt(bpy) fragment to the LUMO is almost negligible for **3'**$^+$. The NPA spin density of **3'**$^+$ was localized exclusively on the Fc fragments. Notably, the contribution of the Fc fragment to the LUMO in **3'**$^+$ increased by 57.5% compared with that of the HOMO in Pt(bpy)(FcC); a contribution to HOMO is largest in the C fragment for **3'** (77%), while a contribution to LUMO is largest in the Fc fragment for **3'**$^+$ (69.5%). Accordingly, the LUMO properties and charge distributions for **3'**$^+$ are different from those for the reference

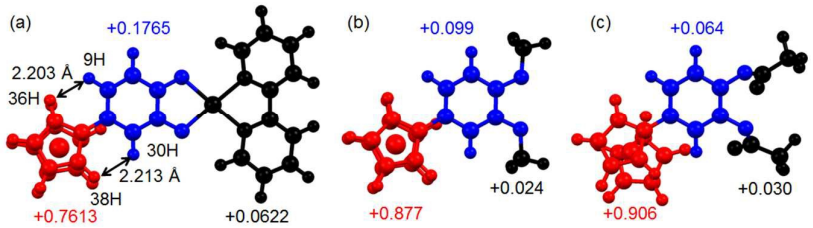

Figure 4. DFT-optimized structures of (a) **3'**$^{+}$, (b) **1**$^{+}$, and (c) **5**$^{+}$ with selected H···H distances. Increased values of NPA charges of Fc (red), oxolene (blue), and X (black) fragments upon one-electron-oxidation from the neutral forms are also shown.

Table 2. DFT-calculated NPA charges of fragments with IEFPCM (CH_2Cl_2).[a]

Compound	Fc	$C_6H_3O_2$	bpy	Pt
3'	–0.0483	–0.7985	0.2217	0.6251
3'$^{+}$	0.713 (0.994)	–0.622 (0.006)	0.256 (0.000)	0.653 (0.000)
Pt(bpy)(C)	-	–0.816	0.188	0.628
[Pt(bpy)(C)]$^{\bullet+}$	-	–0.101 (0.948)	0.370 (0.012)	0.731 (0.040)
1	–0.021	–0.637	0.658[b]	-
1^{+}	0.856 (1.025)	–0.538 (–0.025)	0.682[b] (0.000[b])	-
5	0.008	–0.534	0.526[b]	-
5^{+}	0.914 (1.0072)	–0.470 (–0.0071)	0.556[b] (–0.0001[b])	-

[a]NPA spin densities are also shown in parentheses. [b]Charge and spin density of X substituent.

Table 3. DFT-calculated frontier molecular orbital compositions (%) with IEFPCM (CH_2Cl_2).

Compound	MO	*E* /eV	Fc	$C_6H_3O_2$	bpy	Pt
3'	121 (LUMO)	–2.51	0	3	91	6
	120 (HOMO)	–4.5	12	77	5	6
3'$^{+}$	120β (LUMO)	–3.35	69.5	10.8	1.2	0.3
	119β (HOMO)	–5.21	13	75	4	8
Pt(bpy)(C)	79 (LUMO)	–2.49	-	3	91	6
	78 (HOMO)	–4.56	-	87	6	7
[Pt(bpy)(C)]$^{\bullet+}$	78β (LUMO)	–4.23	-	88.4	5.5	6.1
	78α (HOMO)	–6.23	-	87.5	3.3	9.3
1	80 (LUMO)	–0.48	62.1	37.2	0.7[b]	-
	79 (HOMO)	–5.23	55.7	42.9	1.5[b]	-
1^{+}	79β (LUMO)	–4.17	99	1	0[b]	-
	78β (HOMO)	–6.07	13	83	4[b]	-
5	94 (LUMO)	–0.83	38.7	58.3	3[b]	-
	93 (HOMO)	–5.27	95	5	0[b]	-
5^{+}	93β (LUMO)	–4.34	99.31	0.67	0.02[b]	-
	92β (HOMO)	–7.01	41.2	56.2	2.6[b]	-

[a]Charge and spin density of a Fc unit with Fe1 center. [b]Charge and spin density of X substituent.

compound [Pt(bpy)(C)]$^{\bullet+}$, in which the largest contribution to LUMO and NPA charges is the C fragment (Figure S16, and Tables 2, 3, and S4).

The NPA charges of **1**$^{+}$ (Figure 4b and Table S6) and **5**$^{+}$ (Figure 4c and Table S5) increased significantly on the Fc fragments when compared with those of **1** and **5**, while the contributions of other fragments were minor (Figure 4b and 4c). This suggested that the first oxidation of **1** and **5** occurred largely on the Fc fragment. Such localization of the positive charges is in agreement with the localization of the LUMO (79β for **1**$^{+}$; 93β for **5**$^{+}$) on the Fc fragment (Table 3 and Figure 5b and 5c). The degree of the localization on the Fc fragment was stronger for **5**$^{+}$ than for **1**$^{+}$ due to the presence of the electron-withdrawing acetyl substituent.

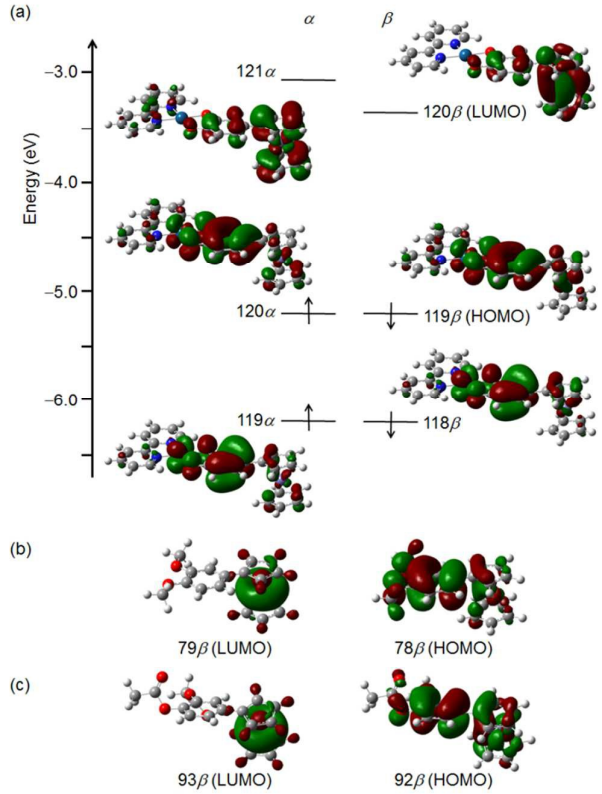

Figure 5. (a) Selected molecular orbital contributions and energy diagrams for **3'**$^{+}$ calculated using a DFT method (isosurface values 0.02 au). Frontier orbitals of (b) **1**$^{+}$ and (c) **5**$^{+}$.

Chemical oxidation of Fc derivatives

To probe the electronic structure and charge distribution of **3**$^{+}$, complex **3** was chemically oxidized using magic blue in CH_2Cl_2. We also chemically oxidized the reference Pt complex, Pt(^{t}Bu$_2$bpy)(C), which was monitored using UV-vis-NIR spectroscopy (Figure S7). The resulting radical cation, [Pt(^{t}Bu$_2$bpy)(C)]$^{\bullet+}$, displayed two absorption bands at 457 and 596 nm. An analogous Pt complex, Pt(dpphen)(^{t}Bu$_2$C) (dpphen = 4,7-diphenyl-1,10-phenanthroline; ^{t}Bu$_2$C = 3,5-di-*tert*-butylcatechol), was reported to be oxidized on the center of the

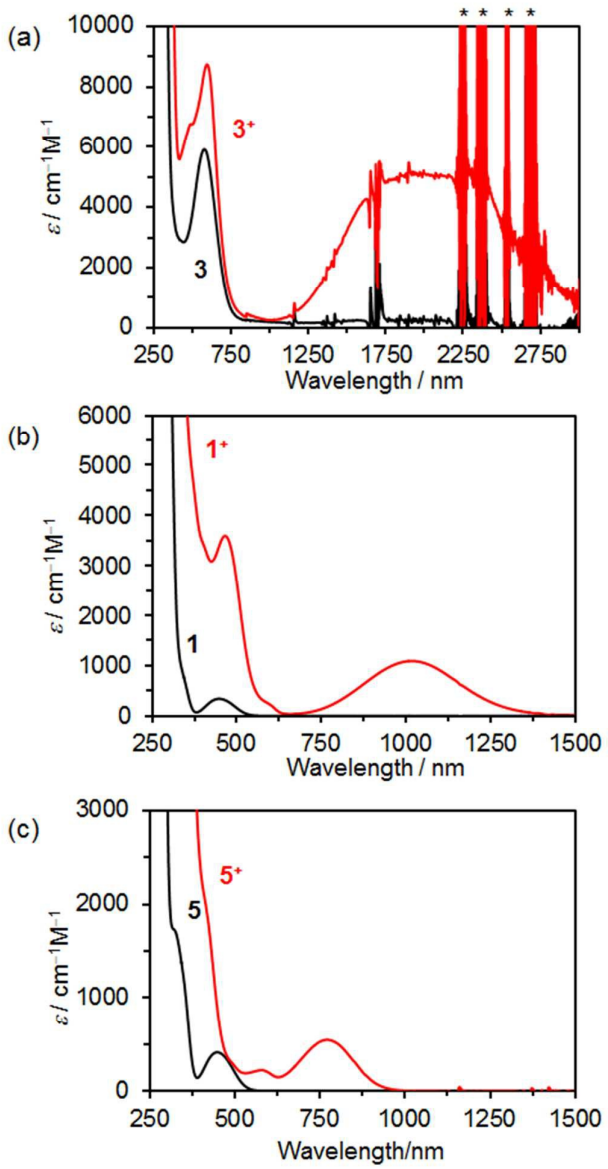

Figure 6. UV-vis-NIR spectra of (a) **3**, (b) **1**, and (c) **5** in the absence (black line) and presence of 1 equiv. of magic blue (red line) in CH_2Cl_2 (* = solvent peaks).

catechol ligand. $[Pt(dpphen)(^tBu_2C)]^{\bullet+}$ also displayed a band at 457 nm, which was assigned to a d(π)-π* MLCT transition, where the π and π* orbitals were based on the SQ ligand.[11b] $[Pt(^tBu_2bpy)(^tBu_2C)]^{\bullet+}$ was also reported to exhibit absorption bands characteristic of a coordinated SQ radical.[11d] Similarly, the oxidation of $Pt(^tBu_2bpy)(C)$ was centered on the catecholate ligand. Indeed, TD-DFT calculations predicted the presence of electronic transitions at 479 nm corresponding to the 75β-78β transition, where 78β (LUMO) based on the SQ ligand serves as the acceptor orbital (Figure S16 and Table S7).

The monocation $\mathbf{3}^+$ displayed two different bands from those observed for $[Pt(^tBu_2bpy)(C)]^{\bullet+}$ (Figure 6a); an intense band at 594 nm in the visible region and a broad band at 1947 nm in the NIR region. Thus, $\mathbf{3}^+$ can be described as Fc^+-centered rather than SQ ligand-centered. This description was in agreement with the DFT calculations for $\mathbf{3}^+$, where the contribution of the Fc moiety to the positive charge and spin density was largest. Indeed, TD-DFT calculations predicted the presence of electronic transitions, where 120β (LUMO) serves as the acceptor orbital in the visible region (Table S7). The predicted transitions are close to the first absorption band observed for $\mathbf{3}^+$ (Figure 6a). The second absorption band observed for $\mathbf{3}^+$ was assigned to an ICT transition from the catecholate moiety to the Fc^+ center, as neither Fc^+ or $[Pt(^tBu_2bpy)(C)]^{\bullet+}$ exhibit absorption bands in the NIR region. Indeed, TD-DFT calculations predicted the presence of an electronic transition from the 119β (HOMO) to 120β (LUMO) at 1396 nm (Table S7). It was demonstrated that a strong NIR absorption band was observed for a binuclear Pt(II) diimine bis-catecholate complex in the mixed-valence catecholate/semiquinone state.[11d] Such spectroscopic properties are similar to those for $\mathbf{3}^+$, indicating a common feature of ligand-based charge transfer transitions in catecholate conjugates.

According to a previously reported method,[8d, 8e] partial chemical oxidation of **3** was performed with substoichiometric amounts of iodine (I_2) in $CDCl_3$ at 294K, which was monitored using ^{1}H-NMR spectroscopy (Figure S18). The proton signals of the Fc and $C_6H_3O_2$ moieties were paramagnetically broadened, while those of the bpy moiety were less broadened. This indicated that both the Fc and $C_6H_3O_2$ moieties participated in the first oxidation of **3**, although the locus of oxidation was not discriminated on the NMR timescale.

The chemical oxidation of compounds **1**, **4**, and **5**, was performed using magic blue in CH_2Cl_2. Compound $\mathbf{1}^+$ exhibited two absorption bands at 466 nm and 1018 nm (Figure 6b), which were analogous to those of $\mathbf{3}^+$. The visible band was blue shifted by 4650 cm^{-1}, and decreased in intensity by a factor of 1.9, when compared with the high-energy band of $\mathbf{3}^+$. The NIR band was blue shifted by 4680 cm^{-1}, and its intensity decreased by a factor of 4.8, when compared to the NIR band of $\mathbf{3}^+$. These bands were assigned to an ICT transition between the V moiety and the Fc^+ center, consistent with the DFT calculations which predicted $\mathbf{1}^+$ was Fc^+-centered, and reported absorption data for ferrocenium-polyaromatic dyads containing electron-rich groups.[9c, 14] Indeed, $\mathbf{1}^+$ exhibited a shoulder peak around 600 nm, typical for Fc^+ species.[15] The absorption bands of $\mathbf{5}^+$ were analogous to those of $\mathbf{1}^+$. Complex $\mathbf{5}^+$ exhibited a shoulder peak around 420 nm and an absorption band at 770 nm, assigned to the ICT transitions from the V moiety to the Fc^+ center, as well as an absorption band at 577 nm, assigned to the Fc^+ center (Figure 6c). The UV-vis spectrum for **4** in the presence of magic blue was similar to that for $\mathbf{5}^+$ (Figures S8), implying that the electron-withdrawing strength of the acetoxy group was comparable to that of the hydrogen atom in the Fc^+-benzene backbone. The change in substitution (X group) in complexes **3** (O^-), **1** (CH_3), and **5** ($OCOCH_3$) led to a blue shift for the ICT bands and decreased their intensities. This reflected the strength of the electronic coupling between the Fc^+ moiety and the catechol-derivatized backbone.

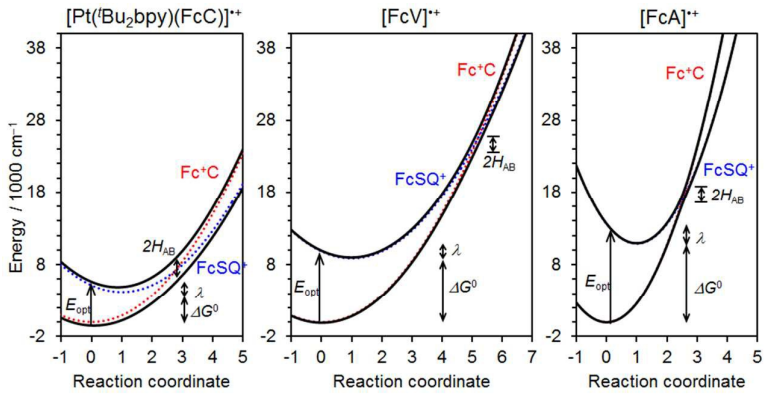

Figure 7. Diabatic (dashed line) and adiabatic (solid line) potential energy surfaces of the Fc^+C and $FcSQ^+$ states for $\mathbf{3}^+$, $\mathbf{1}^+$, and $\mathbf{5}^+$ as a function the electron transfer reaction coordinate.

Table 4. Parameters of ICT bands and electronic coupling.

	$\mathbf{3}^+$		$\mathbf{1}^+$		$\mathbf{5}^+$
$\Delta\upsilon_{1/2}$ (cm^{-1})	3820 [a]	3220 [b]	3720 [a]	3100 [b]	2600 [a]
υ_{max} (cm^{-1})	5140	- [c]	9820	- [c]	12980
ε_{max} ($cm^{-1}M^{-1}$)	5000	- [c]	1040	- [c]	520
r_{DA} (Å)	6.15 [d]	- [c]	4.55 [e]	- [c]	4.42 [e]
H_{AB} (cm^{-1})	1050	980	880	810	620
α [f]	0.20	0.19	0.090	0.082	0.048
ΔG^0 (cm^{-1})	4230	- [c]	8870	- [c]	10270
λ (cm^{-1})	910	- [c]	950	- [c]	2710

[a] Gaussian-fitted values (see Figures S10 to S12). [b] Observed values. [c] Same as the left. [d] The distance between Fe atom and the center of C-C-C-O of the catecholate moiety. [e] The distances between Fe atom and the center of the phenyl ring. [f] Delocalization parameter $\alpha = H_{AB}/\upsilon_{max}$.

Electronic coupling and potential energy curves

The spectroscopic parameters, energy (υ_{max}), intensity (ε_{max}), and bandwidth at the full width half maximum ($\Delta\upsilon_{1/2}$) for complexes $\mathbf{3}^+$, $\mathbf{1}^+$, and $\mathbf{5}^+$ (Figures S10, S11, and S12) were determined by Gaussian deconvolution of the NIR bands (Table 4). Using these parameters, the donor-acceptor distance (r_{DA}) derived from the DFT-optimized structure, and eq. 1, a Hush analysis[16] yielded the electronic coupling values (H_{AB}) for each complex (Table 4).[17] The ground state delocalization parameter (α)[18] for $\mathbf{3}^+$ corresponded to those for the weakly coupled class II MV compounds in the Robin and Day classification.[19] The H_{AB} values increased as the electron-donating strength of the substituents[13] on the phenyl rings increased ($OCOCH_3$ < OCH_3 < O^-). This order correlated to the extent of electronic delocalization as the α value for $\mathbf{3}^+$ was a factor of 2.2 larger than for $\mathbf{1}^+$, while the α value for $\mathbf{1}^+$ was a factor of 1.9 larger than for $\mathbf{5}^+$. This indicated that the degree of electronic communication in the FcC-derivatized backbone can be tuned by chemical substitution of the X group. In particular, metal complexation with the Pt(II) ion dramatically increased the degree of charge delocalization between the organometallic center (Fc) and the catechol-derivatized backbone. Notably, the order of the H_{AB} and α values ($\mathbf{5}^+$ < $\mathbf{1}^+$ < $\mathbf{3}^+$) remained unchanged when $\Delta\upsilon_{1/2}$ was replaced by the observed, rather than the Gaussian-fitted, value.

$$H_{AB} = 0.0206(\upsilon_{max}\,\varepsilon_{max}\,\Delta\upsilon_{1/2})^{1/2}/\,r_{DA} \quad (1)$$

$$h\upsilon_{max} = \Delta G^0 + \lambda \quad (2)$$

The reorganization energy (λ) for complexes $\mathbf{1}^+$, $\mathbf{3}^+$, and $\mathbf{5}^+$ is given by eq. 2, where ΔG^0 denotes the zero-level energy difference between the ground and excited states. The ΔG^0 values can be determined by the difference between the redox potentials (Table 4). Potential energy diagrams for these complexes were constructed based on a two-state Hush model using the parameters listed in Table 4. The diabatic energy surfaces, with the parabolic functions λx^2 and $\lambda(1-x)^2 + \Delta G^0$, are shown in Figure 7. The adiabatic energy surfaces are constructed according to Ref 16b. The ground state of complexes $\mathbf{1}^+$, $\mathbf{3}^+$, and $\mathbf{5}^+$ is the Fc^+C configuration, while the ICT state is the $FcSQ^+$ configuration (Chart 1b). The ΔG^0 value for $\mathbf{1}^+$ was comparable to that of $\mathbf{5}^+$, while the λ value for $\mathbf{1}^+$ was a factor of 2.9 smaller than that of $\mathbf{5}^+$. Accordingly, the two parabolas for $\mathbf{5}^+$ were deeper than those of $\mathbf{1}^+$. The ΔG^0 value for $\mathbf{3}^+$ was a factor of 2.1 smaller than that of $\mathbf{1}^+$ while the λ value for $\mathbf{3}^+$ was only 40 cm^{-1} smaller than that of $\mathbf{1}^+$. Accordingly, the depth of the two parabolas for $\mathbf{3}^+$ was comparable to those of $\mathbf{1}^+$, while the gap between the two parabolas for $\mathbf{3}^+$ (ΔG^0) was smaller than for $\mathbf{1}^+$. The potential energy surfaces of the Fc^+ derivatives can be dramatically modulated by changing the energy level of the molecular orbitals of the appended catechol-derivatized moieties. These findings came from the ease of chemical modification at the O atoms not only by changing the substitution groups but also by metal complexation in the present Fc-conjugate system.

Crystal structures of FcV^+, $FcVFc^+$, and $FcVFc^{2+}$

I_2 is widely used as a weak oxidant for preparative oxidation of Fc derivatives (–0.14 V *vs.* Fc^+/Fc in $CH_3CN/n\text{-}Bu_4NPF_6$).[20] Compound **1** was oxidized by I_2 in chloroform to afford brown single crystals. Crystals suitable for XRD analysis had a composition of $[FcV](I_3)$. The structure of the Fc^+ cation is shown in Figure 8 (left). The average distance between Fe1···Cp1A and Fe1···Cp1B was 1.708 Å (Table 5), close to the value reported for the Fc^+ cation (1.70 Å).[21] This indicated that the positive charge of $\mathbf{1}^+$ was localized on the Fc moiety. The benzene and Cp rings were almost coplanar, with a small twist angle of 7.39°, consistent with the DFT-optimized structure of $\mathbf{1}^+$ (Table S6 and Figure 4b). The two Cp rings were tilted at 10.37° to each other.

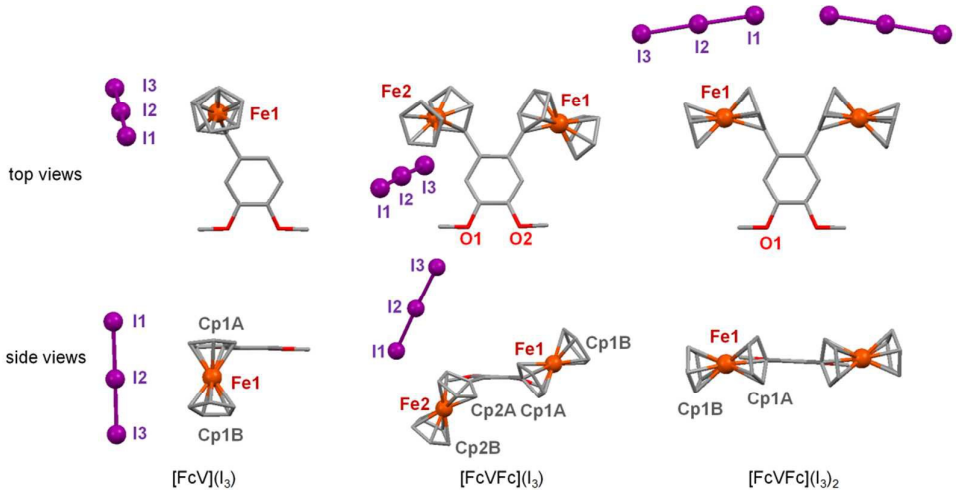

Figure 8. Crystal structures of $[FcV](I_3)$, $[FcVFc](I_3)$, and $[FcVFc]_2(I_3)_2$. Hydrogen atoms in all the views are omitted for clarity, as well as iodine atoms in the side view of $[FcVFc](I_3)_2$.

Table 5. Selected bond lengths (Å) and angles (deg) of $[FcV](I_3)$, $[FcVFc](I_3)$, and $[FcVFc](I_3)_2$.[a]

Compound	$[FcV](I_3)$	$[FcVFc](I_3)$	$[FcVFc](I_3)_2$	FcVFc
Fe1···Fe2	-	6.691	6.879	6.715
Fe1···Cp1A	1.704	1.652	1.708	1.647
Fe1···Cp1B	1.712	1.651	1.715	1.646
Fe2···Cp2A	-	1.710	1.708	1.651
Fe2···Cp2B	-	1.714	1.715	1.652
I1-I2	2.9085(4)	2.93420(17)	2.8945(4)	-
I2-I3	2.9421(3)	2.90894(17)	2.9391(4)	-
I1-I2-I3	178.876(10)	177.676(6)	178.835(14)	-
	this work	this work	this work	Ref. 10

[a]CpXA and CpXB (X = 1, 2) denote the centroids of the Cp rings having compositions of C_5H_4 and C_5H_5, respectively.

Compound **2** was oxidized by I_2 in chloroform to afford both light and deep brown single crystals suitable for XRD analysis. The structure of the former crystals had a composition of $[FcVFc](I_3)$ (Figure 8, middle). The average distance between Fe1···Cp1A and Fe1···Cp1B was 1.6515 Å, close to the reported value of Fc (1.65 Å),[22] while the average distance between Fe2···Cp2A and Fe2···Cp2B was 1.712 Å, close to the reported value of Fc^+ (1.70 Å).[21] These results indicated that the positive charge in $FcVFc^+$ was localized on the Fc moiety of Fe2, and that the $\mathbf{2}^+$ salt was in a valence-trapped state in the crystals. Steric constrains between the Fc and Fc^+ groups increased the twist angles between the benzene and Cp rings (52.93° for Fe1 and 38.11° for Fe2). Both the Fc and Fc^+ groups were in a near eclipsed conformation. The Cp rings were almost parallel to each other, with dihedral angles of 3.99° and 4.00° for Fe 1 and Fe2, respectively.

The structure of the latter crystals, having a composition of $[FcVFc](I_3)_2$, is shown in Figure 8 (right). The two Fc^+ groups were crystallographically equivalent. The average distance between Fe···Cp was 1.7115 Å, close to the reported value for the Fc^+ cation (1.70 Å).[22] The Fc^+ groups were in a near staggered conformation, while the Cp rings were almost parallel to each other (5.397°). The twist angle between the benzene and Cp rings was greater (80.287°) than those of both the neutral form (32.06° for Fe1 and 52.65° for Fe2) and the monocation form (52.93° for Fe1 and 38.11° for Fe2), presumably because of packing-effects with I_3^-. To the best of our knowledge, this is the first crystallographic study of diferrocenyl complexes, which described the structural differences among the three different oxidation states (*i.e.*, the neutral, cationic, and dicationic forms).

Characterization of $FcVFc^+$

The optimized geometry of the diferrocenyl complex in the one-electron oxidized form ($\mathbf{2}^+$) was calculated using DFT calculations. The phenyl and Cp rings were twisted because of steric constrains between the Fc and Fc^+ groups (Figure S17), consistent with the crystal structure. The NPA charges of the Fc1 and Fc2 fragments in $\mathbf{2}^+$ increased by 0.026 and 0.883, respectively, when compared to those of **2**, while those of the V fragment increased by 0.069 (Table S8). This indicated that the positive charge of $\mathbf{2}^+$ was localized largely on the Fc2 fragment. The NPA spin density of $\mathbf{2}^+$ was localized exclusively on the Fc2 fragment (Table S8). The localization of the charge and spin density was in agreement with the localization of the LUMO (121β) on the Fc2 fragment (Figure S18 and Table S9). The localization of the charges resembled to the valence-trapped state in the crystals (Figure 8, middle).

The UV-vis spectrum of $\mathbf{2}^+$ (Figure S9) was analogous to that of the monoferrocenium complex $\mathbf{1}^+$, with the exception that $\mathbf{2}^+$ exhibited a weak NIR band which extended to 2250 nm (Figure S13 and Table S2). This band was assigned to an intervalence charge transfer (IVCT) transition as it was similar to that reported for the mixed-valence species *o*-diferrocenylbenzene.[23]. The H_{AB} value determined for the IVCT was comparable to that of the mixed-valence species *o*-diferrocenylbenzene (H_{AB} = 202 in acetonitrile).[23] This indicated that the inter-ferrocenyl electronic interaction, which occurred through the *ortho* connection in the phenyl ring, was not noticeably affected by the electron-donating strength of the substituents in the 4- and

5-positions. This was in contrast to the large effect that varying substituent had on the H_{AB} and α values for ICT transition in the monoferrocenyl complexes $\mathbf{1}^+$, $\mathbf{3}^+$, and $\mathbf{5}^+$. The H_{AB} value determined for the ICT transition in $\mathbf{2}^+$ was a factor of 1.8 smaller than that in $\mathbf{1}^+$, presumably because the planarity between the Cp and phenyl rings in $\mathbf{1}^+$ was lower than $\mathbf{2}^+$. Potential energy diagrams, corresponding to the IVCT and ICT transitions observed for $\mathbf{2}^+$ (Figure S14), were constructed based on a two-state Hush model and the λ and ΔG^0 parameters. The λ value for the ICT transition in $\mathbf{2}^+$ was a factor of 1.4 smaller than that of $\mathbf{1}^+$, reflecting the difference in size between the cations.

Conclusions

The novel Pt diimine complex Pt(^{t}Bu$_2$bpy)(FcC) (**3**), incorporating the valence tautomeric ligand 4-ferrocenylcatechol, was synthesized and characterized using ^{1}H- and ^{13}C-NMR spectroscopy, ESI-MS, and electrochemical measurements. The ICT behavior and charge distributions of $\mathbf{3}^+$ were explained by comparison with related Fc complexes. DFT calculations and UV-vis-NIR spectroscopy revealed that the cationic complexes $\mathbf{1}^+$, $\mathbf{3}^+$, and $\mathbf{5}^+$, were Fc^+-centered rather than SQ ligand-centered. These complexes exhibited ICT transition bands from the catechol-derivatized framework to the Fc^+ moiety in the NIR region. The H_{AB} and α values increased as the electron-donating strength of the substituent groups of the catechol-derivatized framework increased ($OCOCH_3$ ($\mathbf{5}^+$) < OCH_3 ($\mathbf{1}^+$) < O^- ($\mathbf{3}^+$)). The electronic interactions between the organometallic center and non-innocent framework were tuned by changing the energy level of the molecular orbitals of the catechol-derivatized framework. In contrast, the inter-ferrocenyl electronic interaction, which occurred through *ortho* π-conjugation in the phenyl ring, was not noticeably affected by the electron-donating strength of the substituents in the 5- and 6-positions.

Experimental

Materials and methods

All solvents and chemicals used in the syntheses were of reagent grade and were used without further purification. Ferrocenyl compounds (FcV,[10] FcVFc,[10] and FcB[24]), $PtCl_2(^t$Bu$_2$bpy),[25] and Pt(^{t}Bu$_2$bpy)(C)[11a] were synthesized according to previously reported procedures. Magic blue, (tris(4-bromophenyl)aminium hexachloridoantimonate, purity: > 97.0%), was purchased from Sigma-Aldrich. Tetra-*n*-butylammonium phosphate (^{n}Bu$_4$NPF$_6$) (purity: > 98.0%) was purchased from Tokyo Kasei Kogyo (TCI) and recrystallized from methanol before use.

The ^{1}H- and ^{13}C{^{1}H} spectra were recorded using JEOL JNM-ECP400 and JNM-ECA600 spectrometers installed at the Nara Institute of Science and Technology; tetramethylsilane (TMS) was used as an internal standard (0 ppm) for ^{1}H- and ^{13}C{^{1}H}-NMR analysis. The ESI-MS were obtained using a JEOL JMS-T100CS spectrometer. 1D ^{1}H-NMR differential NOE spectra were recorded using JEOL JNM-ECA600 spectrometers. The UV-vis-NIR absorption spectra were measured on a JASCO V-670 spectrometer at room temperature.

All voltammetric experiments were carried out using a BAS electrochemical analyzer (Bioanalytical Systems Inc, West Lafayette, IN, USA). All experiments were performed using a conventional three-electrode system at 298 K. A platinum wire (1.6 mm diameter) was employed as the counter electrode, a glassy carbon electrode (3.0 mm diameter) as the working electrode and an Ag-AgCl (3.0 M NaCl) electrode as the reference electrode. Typically, nonaqueous CH_2Cl_2 solutions containing **3** and ^{n}Bu$_4$NPF$_6$ (0.1 M) were deaerated prior to each measurement, and an argon atmosphere was maintained inside the cell throughout each measurement. Each experiment was first performed in the absence of any internal standard and then repeated in the presence of decamethylferrocene (Fc*). A separate experiment containing only ferrocene and decamethylferrocene was also performed. The potentials are quoted relative to Fc^{*+}/Fc* couple. In this setup, the Fc^+/Fc couples were observed at 560 mV *vs.* Fc^{*+}/Fc* while the Fc^+/Fc couples were at 664 mV *vs.* Ag/AgCl in CH_2Cl_2/^{n}Bu$_4$NPF$_6$. The potential data quoted relative to the Fc^+/Fc couple are also shown in Table S1.

Synthesis of Pt(^{t}Bu$_2$bpy)(FcC) (3)

FcV (0.300 g, 1.02 mmol) was dissolved in dry degassed dichloromethane (30 mL) and cooled to 0 °C. A dichloromethane solution of BBr_3 (1.0 M, 3 mL) was then added to the solution. After stirring for 30 min at 0 °C and then 30 min at room temperature, the starting material was completely converted, as confirmed by TLC. Degassed water (20 mL) was then added to the reaction mixture using a dropping funnel. After stirring vigorously for 10 min, the organic phase was obtained using a phase separator filter and concentrated to dryness. The obtained crude product of 4-ferrocenylcatechol (0.220 g) was treated with $NaHCO_3$ (0.125 g, 1.48 mmol) and $PtCl_2(^t$Bu$_2$bpy) (0.400 g, 0.740 mmol) in dry ethanol (20 mL) and dry DMF (4 mL) under N_2 atmosphere at 95 °C for 24h. A dark purple solid was reprecipitated upon addition of H_2O to the concentrated reaction mixture. The solid was obtained by filtration and washed with water and ether. The obtained solid was purified by silica-gel column chromatography (Wakogel C-300) using chloroform/methanol (99/1) to remove the unreacted $PtCl_2(^t$Bu$_2$bpy) and chloroform/methanol (98/2) to recover the product as a major purple fraction. The target product was obtained by washing with *n*-hexane. Yield: 400 mg (71%). ^{1}H-NMR (600 MHz, $CDCl_3$, ppm): δ = 1.45 (s, 18H, C$\underline{H}_3$), 1.46 (s, 18H, C$\underline{H}_3$), 4.02 (s, 5H, $C_{Cp}(3)\underline{H}$), 4.17 (pt, 4H, $C_{Cp}(2)\underline{H}$), 4.58 (pt, 4H, $C_5\underline{H}_4$), 6.64 (dd, J = 1.8, 7.7 Hz, 1H, $C_{Ph}(5)\underline{H}$), 6.70 (d, J = 7.7 Hz, 1H, $C_{Ph}(6)\underline{H}$), 6.97 (d, J = 1.8 Hz, 1H, $C_{Ph}(2)\underline{H}$), 7.45 (m, 2H, $C_{bpy}\underline{H}$), 7.78 (m, 2H, $C_{bpy}(3)\underline{H}$, $C_{bpy}(3')\underline{H}$), 9.16 (m, 2H, $C_{bpy}\underline{H}$) (Figure S2). ^{13}C-NMR (150 MHz, $CDCl_3$, ppm): δ = 30.27($C(\underline{C}H_3)_3$), 35.83, 35.85, 65.65 ($\underline{C}_{Cp}(2)$), 67.55($\underline{C}_{Cp}(3)$), 69.37 ($\underline{C}_5H_5$), 88.23, 112.57 ($\underline{C}_{Ph}(3)$), 114.06 ($\underline{C}_{Ph}(6)$), 115.08 ($\underline{C}_{Ph}(5)$), 119.09 ($\underline{C}_{py}(3)$), 119.14 ($\underline{C}_{py}(3)$), 123.88, 123.93, 149.08, 149.13, 155.91, 155.94, 161.7, 162.33, 162.58 (Figure S3). UV-vis (CH_2Cl_2): [λ_{max}/nm], 578 (1.73×10^5). HR-ESI-

MS (*m/z*). Calc. for $C_{34}H_{26}FeN_2O_2Pt$ ($[M]^+$): 755.17739. Found: 755.17718 (Figure S1).

Synthesis of FcA (5)

The crude product of 4-ferrocenylcatechol (0.0500 g), prepared by the same procedures as those for synthesis of **3**, was treated with pyridine (2 mL) and acetic anhydride (1 mL) under N_2 atmosphere. After stirring at room temperature for 12 h, dry dichloromethane (10 mL) was added to the reaction mixture. The organic phase was washed with water (30 mL × 2) and brine (30 mL) and concentrated to dryness. The obtained solid was purified by silica-gel column chromatography (Wakogel C-300) using dichloromethane as the eluent. Yield: 20 mg (28%). ^{1}H-NMR (600 MHz, $CDCl_3$, ppm): δ = 2.30 (s, 3H, C$\underline{H}_3$), 2.32 (s, 3H, C$\underline{H}_3$), 4.07 (s, 5H, $C_5\underline{H}_5$), 4.31 (pt, 2H, $C_{Cp}(3)\underline{H}$), 4.57 (pt, 2H, $C_{Cp}(2)\underline{H}$), 7.10 (d, J = 8.3 Hz, 1H, $C_{Ph}(6)\underline{H}$), 7.27 (d, J = 2.1 Hz, 1H, $C_{Ph}(3)\underline{H}$), 7.33 (dd, J = 8.3, 2.1 Hz, 1H, $C_{Ph}(5)\underline{H}$) (Figure S4). ^{13}C-NMR (150 MHz, $CDCl_3$, ppm): δ = 20.74 (O$\underline{C}H_3$), 20.72 (O$\underline{C}H_3$), 66.74 ($\underline{C}_{Cp}(2)$), 69.11 ($\underline{C}_{Cp}(3)$), 69.67 ($\underline{C}_5H_5$), 84.06, 121.04 ($\underline{C}_{Ph}(3)$), 123.10 ($\underline{C}_{Ph}(6)$), 124.12 ($\underline{C}_{Ph}(5)$), 138.60, 139.99, 142.91, 168.40 ($\underline{C}$=O), 168.31 ($\underline{C}$=O) (Figure S5). HR-ESI-MS (*m/z*). Calc. for $C_{20}H_{18}FeO_4$ ($[M]^+$): 378.05545. Found: 378.05509 (Figure S1).

DFT calculation data

The DFT calculations were carried out using the Gaussian09 program package.[26] For the Pt complexes (**3** and **3'**$^+$), the ^{t}Bu$_2$bpy group was replaced by bpy to afford **3'** and **3''**$^+$. The restricted or unrestricted three-parameterized Becke–Lee–Yang–Parr (B3LYP or UB3LYP) hybrid exchange-correlation functional[27] was used with the Lanl2DZ (Hay–Wadt ECP) basis set[28] for the Fe and Pt atoms and the 6-31G(d) basis set[29] for the other atoms with taking account of solvent effects. The solvent effects of CH_2Cl_2 were modeled using IEFPCM.[30] The stability of the optimized structures was confirmed by calculating the molecular vibrational frequencies, in which no imaginary frequencies were observed. Molecular orbital composition analysis was conducted using the GaussSum Program. The TD-DFT method was used to calculate transition energies and oscillator strengths relevant to the absorption spectra.

Single crystal X-ray diffraction (XRD) analysis

Oxidized form of FcV: To a $CHCl_3$ solution of I_2 FcV was added. To the resulting solution *n*-hexane was added and kept at room temperature. After the reprecipitate was washed with *n*-hexane, the target compound was obtained as brown rod crystals having a composition of [FcV](I_3). *Oxidized forms of FcVFc*: To a $CHCl_3$ solution of I_2 FcVFc was added. To the resulting solution *n*-hexane was added and kept at room temperature. After the reprecipitate was washed with *n*-hexane, the target compound was obtained as light brown crystals having a composition of [FcVFc](I_3) and dark brown crystals having a composition of [FcVFc](I_3)$_2$.

Data were collected with a Rigaku ValiMax RAPID RA-Micro7HFM using Mo Kα radiation. The diffraction data were processed with RAPID AUTO on a Rigaku program, and the structures were solved by direct methods and refined on F^2 by full-matrix least-squares using CrystalStructure and SHELXL-97. The CCDC numbers in Table S10 contain the supplementary crystallographic data for this paper. These data can be obtained free of charge from the Cambridge Crystallographic Data Centre via www.ccdc.cam.ac.uk/data_request/cif.

Acknowledgements

This work was partially supported by a Grant-in-Aid for Young Scientists B (No. 25790016) and a research grant from the Murata Science Foundation. The authors would like to thank Mr. Fumio Asanoma and Ms. Yoshiko Nishikawa (NAIST) for the NMR and ESI-MS measurements, respectively.

Notes and references

1 For selected reviews, see: (a) E. Evangelio and D. Ruiz-Molina, *Eur. J. Inorg. Chem.*, 2005, 2957-2971; (b) W. Kaim, *Inorg. Chem.*, 2011, **50**, 9752-9765; (c) D. Michael and P. Mingos, *J. Organomet. Chem.*, 2014, **751**, 153-173.

2 For selected reviews, see: (a) P. Gütlich and A. Dei, *Angew. Chem. Int. Ed. Engl.*, 1997, **36**, 2734-2736. (b) C. G. J. Pierpont, *Coord. Chem. Rev.*, 2001, ***216-217***, 99-125. (c) C. G. J. Pierpont, *Coord. Chem. Rev.*, 2001, ***219-221***, 415-433; (d) A. Dei, D. Gatteschi, C. Sangregorio and L. Sorace, *Acc. Chem. Res.*, 2004, **37**, 827-835; (e) O. Sato, A. Gui, R. Matsuda, J. Tao and S. Hayami, *Acc. Chem. Res.*, 2007, **40**, 361-369.

3 R. M. Buchanan and C. G. J. Pierpont, *J. Am. Chem. Soc.*, 1980, **102**, 4951-4957.

4 H.-C. Chang and D. Kiriya, *Eur. J. Inorg. Chem.*, 2013, 642-652.

5 (a) M. Nihei, Y. Sekine, N. Suganami, K. Nakazawa, A. Nakao, H. Nakao, Y. Murakami and H. Oshio, *J. Am. Chem. Soc.*, 2011, **133**, 3592-3600; (b) T. Matsumoto, G. N. Newton, T. Shiga, S. Hayami, Y. Matsui, H. Okamoto, R. Kumai, Y. Murakami and H. Ohio, *Nat. Commun.*, 2014, **5**, 3865/1-3865/8.

6 D. Kiriya, K. Nakamura, H.-C. Chang and S. Kitagawa, *Chem. Commun.*, 2009, 4085-4087.

7 For selected reviews of biferrocene, see: (a) D. O. Cowan, C. LeVanda, J. Park and F. Kaufman, *Acc. Chem. Res.*, 1973, **6**, 1-7; (b) D. Astruc, *Acc. Chem. Res.*, 1997, **30**, 383-391; (c) H. Nishihara, *Bull. Chem. Soc. Jpn.*, 2001, **74**, 19-29. For a selected review of Fc-porphyrin conjugates, see: (d) C. Bucher, C. H. Devillers, J.-C. Moutet, G. Royal and S.-A. Eric, *Coord. Chem. Rev.*, 2009, **253**, 21-36.

8 For selected recent examples of Fc conjugates, see: (a) I. Ratera, C. Sporer, D. Ruiz-Molina, N. Ventosa, J. Baggerman, A. M. Brouwer, C. Rovira and J. Veciana, *J. Am. Chem. Soc.*, 2007, **129**, 6117-6129. (b) T. Kusamoto, K. Takada, R. Sakamoto, S. Kume and H. Nishihara, *Inorg. Chem.*, 2012, **51**, 12102-12113. (c) T. Kusamoto, H. Nishihara and R. Kato, *Inorg. Chem.*, 2013, **52**, 13809-13811. (d) K. Heinze and S. Reinhardt, *Organometallics*, 2007, **26**, 5406-5414. (e) H. Huesmann, C. Förster, D. Siebler, T. Gasi and K. Heinze, *Organometallics*, 2011, **31**, 413-427.

9 (a) M. Murata, M. Yamada, T. Fujita, K. Kojima, M. Kurihara, K. Kubo, Y. Kobayashi and H. Nishihara, *J. Am. Chem. Soc.*, 2001, **123**, 12903-12904. (b) S. Fukuzumi, Y. Yoshida, K. Okamoto, H. Imahori, Y. Araki and O. Ito, *J. Am. Chem. Soc.*, 2002, **124**, 6794-6795. (c) S. B. Colbran, S. T. Lee, D. G. Lonnon, F. J. D. Maharaj, A. M. McDonagh, K.

A. Walker and R. D. Young, *Organometallics*, 2006, **25**, 2216-2224. (d) A. Neidlinger, V. Ksenofontov and K. Heinze, *Organometallics*, 2013, **32**, 5955-5965.
10 K. Tahara, T. Akita, S. Katao and J. Kikuchi, *Dalton Trans.*, 2014, **43**, 1368-1379.
11 (a) S. S. Kamath, V. Uma and T. S. Srivastava, *Inorg. Chim. Acta*, 1989, **166**, 91-98. (b) J. A. Weinstein, M. T. Tierney, E. S. Davies, K. Base, A. A. Robeiro and M. W. Grinstaff, *Inorg. Chem.*, 2006, **45**, 4544-4555. (c) N. M. Shavaleev, E. S. Davies, H. Adams, J. Best and J. A. Weinstein, *Inorg. Chem.*, 2008, **47**, 1532-1547. (d) J. Best, I. V. Sazanovich, H. Adams, R. D. Bennett, E. S. Davies, A. J. H. M. Meijer, M. Towrie, S. A. Tikhomirov, O. V. Bouganov, M. D. Ward and J. A. Weinstein, *Inorg. Chem.*, 2010, **49**, 10041-10056. (e) H.-C. Chang, K. Komasaka, K. Kishida, T. Shiozaki, T. Ohmori, T. Matsumoto, A. Kobayashi, M. Kato and S. Kitagawa, *Inorg. Chem.*, 2011, **50**, 4279-4288.
12 The reported first and second oxidation potential values for Pt(bpy)(C) is 450 mV and 700 mV vs. Ag-AgCl in acetonitrile. See ref 11a.
13 C. Hansh, A. Leo and R. W. Taft, *Chem. Rev.*, 1991, **91**, 165-195.
14 L. Cuffe, R. D. A. Hudson, J. F. Gallagher, S. Jennings, C. J. McAdam, R. B. T. Connelly, A. R. Manning, B. H. Robinson and J. Simpson, *Organometallics*, 2005, **24**, 2051-2060.
15 *Inorganic Electronic Spectroscopy*; A. B. P. Lever, eds.; Elsevier: Amsterdam, 1984; pp. 659-671.
16 (a) K. D. Demadis, C. M. Hartshorn and T. J. Meyer, *Chem. Rev.,* 2001, **101**, 2655-2685. (b) B. S. Brunschwig, C. Creutz and N. Sutin, *Chem. Soc. Rev.,* 2002, **31**, 168-184. (c) D. M. D'Alessandro and F. R. Keene, *Chem. Soc. Rev.,* 2006, **35**, 424-440. (d) D. M. D'Alessandro and F. R. Keene, *Chem. Rev.,* 2006, **106**, 2270-2298. (e) P. Aguirre-Etcheverry and D. O'Hare, *Chem. Rev.,* 2010, **110**, 4839-4864.
17 We defined r_{DA} as the distance between Fe atom and the center of C-C-C-O of the catecholate moiety in $\mathbf{3}^{+}$, in consideration of the difficulties in determining the accurate estimation of r_{DA} because of the wide delocalization of the π-orbital in the catecholate moiety.
18 H. Nishihara, *Adv. Inorg. Chem.*, 2002, **53**, 41-86.
19 (a) M. B. Robin and P. Day, *Adv. Inorg. Chem. Radiochem.* 1967, **10**, 247–422. (b) C. Creutz, *Prog. Inorg. Chem.*, 1983, **30**, 1–73. (c) N. S. Hush, *Prog. Inorg. Chem.*, 1967, **8**, 391–444.
20 (a) I. V. Nelson and R. T. Iwamoto, *J. Electroanal. Chem.*, 1964, **7**, 218-221; (b) N. G. Connelly and W. E. Geiger, *Chem. Rev.*, 1996, **96**, 877-910.
21 N. J. Mammano, A. Zalkin, A. Landers and A. L. Rheingold, *Inorg. Chem.*, 1977, **16**, 297-300.
22 P. Seiler and J. D. Dunitz, *Acta Crystallogr., Sect. B*, 1979, **35**, 1068-1074.
23 C. Patoux, C. Coudret, J.-P. Launay, C. Joachim and A. Gourdon, *Inorg. Chem.*, 1997, **36**, 5037-5049.
24 C. Imrie, C. Loubser, P. Engelbrecht and C. W. McCleland, *J. Chem. Soc., Perkin Trans.*, 1999, **1**, 2513-2523.
25 J. Yang, D. K. Kersi, L. J. Giles, B. W. Stein, C. Feng, C. R. Tichnell, D. A. Shultz and M. L. Krik, *Inorg. Chem.*, 2014, **53**, 4791–4793.
26 M. J. Frisch, G. W. Trucks, H. B. Schlegel, G. E. Scuseria, M. A. Robb, J. R. Cheeseman, G. Scalmani, V. Barone, B. Mennucci, G. A. Petersson, H. Nakatsuji, M. Caricato, X. Li, H. P. Hratchian, A. F. Izmaylov, J. Bloino, G. Zheng, J. L. Sonnenberg, M. Hada, M. Ehara, K. Toyota, R. Fukuda, J. Hasegawa, M. Ishida, T. Nakajima, Y. Honda, O. Kitao, H. Nakai, T. Vreven, J. A. Montgomery, Jr., J. E. Peralta, F. Ogliaro, M. Bearpark, J. J. Heyd, E. Brothers, K. N. Kudin, V. N. Staroverov, R. Kobayashi, J. Normand, K. Raghavachari, A. Rendell, J. C. Burant, S. S. Iyengar, J. Tomasi, M. Cossi, N. Rega, J. M. Millam, M. Klene, J. E. Knox, J. B. Cross, V. Bakken, C. Adamo, J. Jaramillo, R. Gomperts, R. E. Stratmann, O. Yazyev, A. J. Austin, R. Cammi, C. Pomelli, J.W. Ochterski, R. L.Martin, K.Morokuma, V. G. Zakrzewski, G. A. Voth, P. Salvador, J. J. Dannenberg, S. Dapprich, A. D. Daniels, Ö. Farkas, J. B. Foresman, J. V. Ortiz, J. Cioslowski and D. J. Fox, Gaussian 09, Gaussian, Inc., Wallingford, CT, 2009.
27 D. Becke, *J. Chem. Phys.*, 1993, **98**, 5648-5652.
28 P. Hay and W.R. Wadt, *J. Chem. Phys.*, 1985, **82**, 270–273.
29 P. C. Hariharan and J. A. Pople, *Theor. Chim. Acta*, 1973, **28**, 213–222.
30 (a) B. Mennucci, E. Cancès, and J. Tomasi, *J. Phys. Chem. B*, 1997, **101**, 10506-10517. (b) J. Tomasi, B. Mennucci and R. Cammi, *Chem. Rev.*, 2005, **105**, 2999–3093.

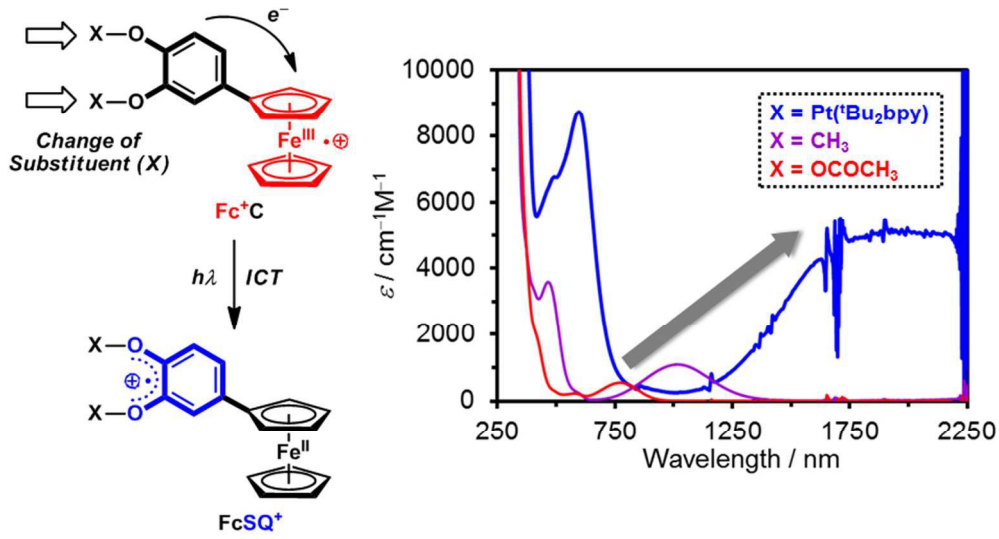

The electronic interactions between an organometallic center and a non-innocent framework were tuned by chemical substitution.
253x133mm (96 x 96 DPI)